CISM COURSES AND LECTURES

The series presents lecture notes, monographs, edited works and proceedings in the field of Mechanics, Engineering, Computer Science and Applied Mathematics.
Purpose of the series is to make known in the international scientific and technical community results obtained in some of the activities organized by CISM, the International Centre for Mechanical Sciences.

INTERNATIONAL CENTRE FOR MECHANICAL SCIENCES

COURSES AND LECTURES - No. 490

THIN FILMS OF SOFT MATTER

EDITED BY

SERAFIM KALLIADASIS
IMPERIAL COLLEGE LONDON, UK

UWE THIELE
MAX-PLANCK- INSTITUT FÜR PHYSIK KOMPLEXER SYSTEME,
DRESDEN, GERMANY

SpringerWienNewYork

This volume contains 84 illustrations

Printed in Italy
SPIN 11975090

All contributions have been typeset by the authors.

ISBN-10 3-211-69807-8 SpringerWienNewYork
ISBN-13 978-3-211-69807-5 SpringerWienNewYork

PREFACE

This book contains lecture notes, albeit not covering all material, delivered at the Advanced Course 'Thin Films of Soft Matter' that took place at CISM Udine in July 18-22, 2005.

Thin film flows of soft matter (either simple Newtonian liquids or polymeric and other complex materials) are often encountered in a wide variety of natural phenomena and technological applications: from gravity currents under water and lava flows to heat and mass transport processes in conventional engineering applications and more recent developments in the area of nanotechnology and MEMS. In the vast majority of cases, thin film flows are bounded by either free surfaces which separate the film from the surrounding phases, as in the case of jets or soap films, or by a free surface and a solid substrate. The involved scales range from the nanometer level as for dewetting thin polymer films and break-up of nanojets to the centimetre scale as for heat and mass transport applications to the meter scale as for lava flows.

The Course aimed at giving a detailed overview of the main and most up-to-date advances in the area of thin films and jets, through a balanced combination of theory and experiments. Since the subject is essentially an interdisciplinary area and as such it brings together scientists and engineers with different educational backgrounds, it was important to offer a research-oriented exposition of the fundamentals of free-surface flows in confined geometries. The goal was to arrive at ready-to-use mathematical models of different degrees of complexity which are capable of describing accurately thin film and jet flows in a relatively 'simple' (i.e. avoiding using the full Navier-Stokes equations) and experimentally testable way.

A wide range of topics was covered: basic equations and interfacial boundary conditions, as well as derivation of model equations for the evolution of the free surface including long-wave expansions and equations of the boundary-layer type; linear stability analyses, weakly and strongly nonlinear analyses including construction of stationary periodic, solitary wave and similarity solutions; interfacial instabilities and formation of complex wave structures; dewetting on chemically homogeneous and heterogeneous substrates; influence of surface tension gradients due to the thermal Marangoni effect and thermocapillary Marangoni instabilities; rupture/dewetting for very thin one- and two-layer films; miscible fingering in electrokinetic flow as a model system to study extended domain dynamics problems, such as the falling film problem, driven by the dominant zero modes associated with key symmetries; influence of chemical reactions and three-dimensional effects on falling liquid films; generic treatment of self-similarity, scaling laws, dimensional analysis and scaling theory of singularities, which is crucial not only

for the specificity of the Course but also from the point of view of general mechanics; singularity formation and topological transitions such as drop break-up and nanojet break-up; experimental characterization of capillarity such as spreading drops, wetting of textured surfaces, wicking and coating; experimental characterization of thin films using atomic force microscopy, ellipsometry and contact angle measurements, and analysis of patterns using Minkowski functionals.

The Course was organized at the suggestion of Professor Manuel G. Velarde, while he was in office as Rector of CISM (2002-2005). It was not a mere suggestion. He provided the organizers (now the editors of this book) with valuable recommendations about topics, names of potential lecturers and an important advice: emphasis on combination of theory, natural phenomena, lab experiments and numerical experiments. This was the natural thing for he had been and still is engaged in the field covered by the Summer School. On the other hand both the present editors had been and still are collaborating with him in some of the themes discussed here. Though Rector of CISM he participated as a student in our School.

Professor Velarde was born in Almeria, Spain, September 7, 1941 and hence he is turning 65 in 2006. He has made seminal and long lasting contributions to fluid physics and, in particular, to our understanding of hydrodynamic instabilities and convective pattern dynamics, wetting and spreading dynamics, interfacial hydrodynamics, and nonlinear wave dynamics. In the latter subfield he is responsible for introducing the concept of 'dissipative soliton' to account for experiments on surface tension gradient-driven waves. In spite of the diversity and heterogeneity of his publications, Professor Velarde has always emphasized the unifying perspective underlying them all. This he taught us to look for in our own research.

We the editors take pleasure in dedicating this book to Professor Manuel G. Velarde on his 65th birthday, with the hope of seeing him again as a student in another of our courses while continuing collaborating with him, a superb teacher.

Manuel G. Velarde amicitiae et admirationis ergo.

The coordinators of the School and editors of this book wish to express their appreciation to Professors Hsueh-Chia Chang, Jens Eggers, David Quéré and Ralf Seemann for their acceptance of both duties, lecturing and writing lecture notes. They specially thank Ioan Vancea for help with the final typesetting. They also acknowledge the CISM Scientific Council for their encouragement and support. Last but not least, they are grateful to the Secretariat staff of CISM and in particular Signora Elsa Venir and Signora Carla Toros for their efficient handling of administrative matters before and during the duration of the School.

Serafim Kalliadasis (London), Uwe Thiele (Dresden)

CONTENTS

SpringerWienNewYork

Structure Formation in Thin Liquid Films: Interface Forces Unleashed

Ralf Seemann,* Stephan Herminghaus,* Karin Jacobs‡

* Max Planck Institute for Dynamics and Self-Organization, Göttingen, Germany
‡ Experimental Physics, Saarland University, Saarbrücken, Germany

Abstract We present a conclusive overview of the stability conditions and the dewetting scenarios of thin liquid coatings. The stability of thin films is given by the effective interface potential $\phi(h)$ of the system and depends among other parameters on the film thickness h. In the case of unstable or metastable films holes will appear in the formerly uniform layer and the film dewets the substrate. We describe the analysis of emerging hole patterns and how to distinguish between different dewetting scenarios. From this analysis we derive the effective interface potential for our particular system, $\phi(h)$, which agrees quantitatively with what is computed from the optical properties of the system. Our studies on thin polystyrene films on Si wafers of variable Si oxide layer thickness demonstrate that the assumption of additivity of dispersion potentials in multilayer systems yields good results and are also in accordance with recent numerical simulations.

Thin liquid films on solid substrates are present in everyday life, e.g. as lubricant film on the cornea of our eyes or on the piston in a car's motor, but also as ink on a transparency. In some cases, these films are not stable on their substrate and bead up, a phenomenon that is easily observable if one tries to paint an oily surface. In recent years, much effort has been put into understanding the dewetting phenomena in thin films on solid substrates, both experimentally (Reiter, 1992; Bischof et al., 1996; Xie et al., 1998; Jacobs et al., 1998a; Herminghaus et al., 1998; Kim et al., 1999; Sferrazza et al., 1998; Seemann et al., 2001b; Tsui et al., 2003; Seemann et al., 2005; Fetzer et al., 2005) and theoretically (Vrij, 1966; Ruckenstein and Jain, 1974; Brochard-Wyart and Daillant, 1989; Sharma and Khanna, 1998, 1999; Konnur et al., 2000; Koplik and Banavar, 2000; Thiele et al., 2001, 2002; Thiele, 2003; Sharma, 2003; Münch, 2005). On the one hand, industry is interested in the prevention of dewetting in order to achieve e.g. stable lithographic resists. On the other hand, basic research is still demanding general rules to infer the rupture and dewetting mechanisms from the spatial ordering and timely evolution of the dewetting pattern. The knowledge of the underlying forces and mechanisms would enable us to predict stability conditions for practical use.

Earlier studies of dewetting scenarios either concentrated on the morphological characterization (Reiter, 1992; Bischof et al., 1996; Xie et al., 1998; Jacobs et al., 1998a) or on the simulation of dewetting patterns on the basis of an assumed effective interface potential (Konnur et al., 2000; Koplik and Banavar, 2000). Some studies took long-range forces into account, but faced the difficulty that their origin and strength was not known precisely (Herminghaus et al., 1998; Kim et al., 1999; Sferrazza et al., 1998). We have therefore studied a model system polystyrene (PS) on silicon (Si) substrates with various silicon oxide (SiO) layers which accounts for all of the important features observed in more complex situations. Owing to the simplicity of the model system we used, a thin film (< 60 nm) of a non-polar liquid on a solid substrate, it is possible to calculate quantitatively the effective interface potential (Israelachvili, 1992) and to compare it to what is derived from the dewetting morphology.

To study dewetting phenomena, a system was used that is on the one hand close to application (coatings, photoresist), yet on the other hand easily controllable in the experiments. Polymers such as polystyrene (PS) are very suitable model liquids since they have a very low vapor pressure in the melt, and mass conservation is valid. Moreover, they are chemically inert, non-polar, and their dynamics can be tailored by choosing different chain lengths and annealing temperatures. Below the glass transition temperature T_g, the film is glassy and can be stored for subsequent analysis. For this work, atactic polystyrene was used due to the known absence of any crystallization in this material.

If not denoted otherwise thin polystyrene films ('PS(2k)', $M_w = 2.05$ kg/mol, $M_w/M_n = 1.05$, Polymer Labs, Church Stratton, UK) were prepared from toluene solution onto three types of silicon wafers: Type A and B with thin natural oxide layer of 1.7 nm or 2.4 nm respectively (Wacker Chemitronics, Burghausen, Germany; (100)-oriented, p-doped, conductivity < 10 Ωcm) and type C with a thick oxide layer of 190(1) nm (Silchem GmbH, Freiberg, Germany; (100)-oriented, p-doped, conductivity > 1 Ωcm). Prior to coating, the silicon wafers were degreased by sonicating them in ethanol, acetone, and toluene. Residual hydrocarbons were etched away by a 30 min dip in fresh 1:1 H_2SO_4 (conc.)/H_2O_2 (30%) solution. Subsequently, the acids were removed by a thorough rinse in hot Millipore^{TM} water.

Cleaning and coating were performed in a class 100 clean room. The thicknesses of the silicon wafers' oxide layer and of the polymer films were measured by ellipsometry (Optrel GdBR, Berlin, Germany). In what follows, we use the term 'SiO' for the silicon oxide layer, despite the fact that most of the amorphous layer consists of silicon dioxide (Sze, 1981). Further characterization of wafers and polymer films was done by atomic force microscopy (AFM) (Multimode III, Digital Instruments, Santa Barbara) using Tapping Mode^{TM}. AFM revealed the rms-roughness of the silicon wafers to be below 0.2 nm, that of the polymer film below 0.3 nm. Samples were annealed on a temperature-controlled hot plate to temperatures between 50 and 140°C for typically 2 to 360 min. AFM scanning parameters were optimized not to affect the liquid polymer films. In some cases, also X-ray diffraction (grazing-incidence diffraction at Troika II, ESRF, Grenoble) was used to determine PS film thickness.

To start with, it is necessary to clarify the distinction between stable, metastable, and unstable films. This is straightforward in terms of the effective interface potential, $\phi(h)$, which is defined as the excess free energy (per unit area) it takes to bring two interfaces

from infinity to a certain distance, h (Dietrich, 1988; Schick, 1989). In our case, the two interfaces involved are the solid/liquid interface and the liquid/air interface, and h_0 is the initial thickness of the liquid film. By definition, $\phi \to 0$ for $h \to \infty$, as shown for three important cases in Figure 1. The solid line (1) characterizes a film that is stable on the substrate, since energy would be necessary to thin the film. The equilibrium film thickness is infinite. The two other curves exhibit a global minimum of $\phi(h)$ at $h = h_{eq}$ and the system can gain energy by changing its present film thickness h to h_{eq}.

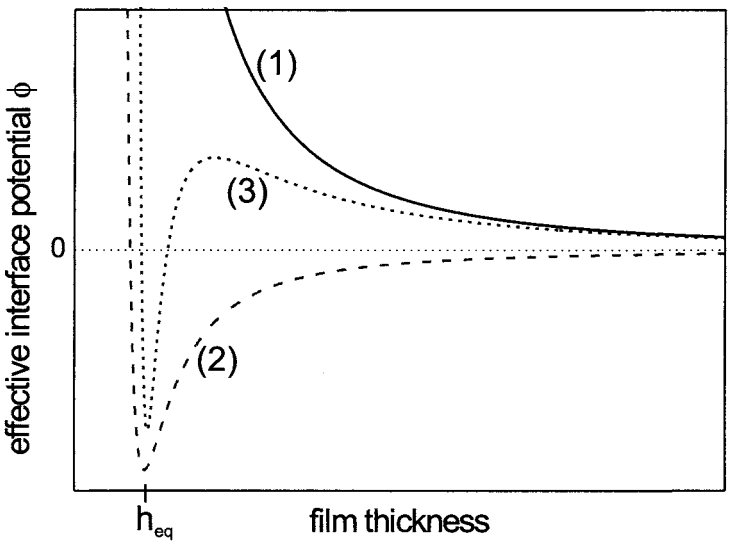

Figure 1. Sketch of the effective interface potential $\phi(h)$ as function of film thickness for a stable (1), unstable (2), and metastable film (3), respectively.

Dewetting is characterized by the formation of circular holes, their growth in time and coalescence, finally leading to a set of droplets on the substrate. A negative global minimum of $\phi(h)$ at a finite film thickness h_{eq} indicates that after dewetting of the film into droplets, an equilibrium layer of thickness h^* will be left on the substrate. The depth of that minimum is connected with the contact angle θ_{eq} of the liquid on the solid substrate (Dietrich, 1988; Schick, 1989; Frumkin, 1938; Seemann et al., 2001d):

$$|\phi(h_{eq})| = \sigma(1 - \cos\theta); \tag{1}$$

where σ is the surface tension of the liquid air interface.

A typical dewetting experiment under lab conditions is shown in Figure 2. Here, two main rupture mechanisms are possible. i) Dry spots are nucleated. Nucleation may be initiated by defects as, e.g., dust particles (heterogeneous nucleation) or by thermal nucleation. ii) Capillary waves are spontaneously amplified. The latter mechanism is

called 'spinodal dewetting' (Vrij, 1966; Ruckenstein and Jain, 1974; Brochard-Wyart and Daillant, 1989). It is readily shown that spinodal dewetting can take place only if the second derivative of ϕ with respect to film thickness is negative, $\phi''(h_0) < 0$, where h_0 is the initial thickness of the homogeneous film. Whenever this is the case, the system is called unstable. Hence, the dashed curve (2) of Figure 1 characterizes an unstable film. The dotted curve (3) describes a film that is unstable for small film thicknesses, where $\phi''(h) < 0$, whereas for larger film thicknesses, only nucleation can drive the system towards dewetting. Here, the film is called metastable.

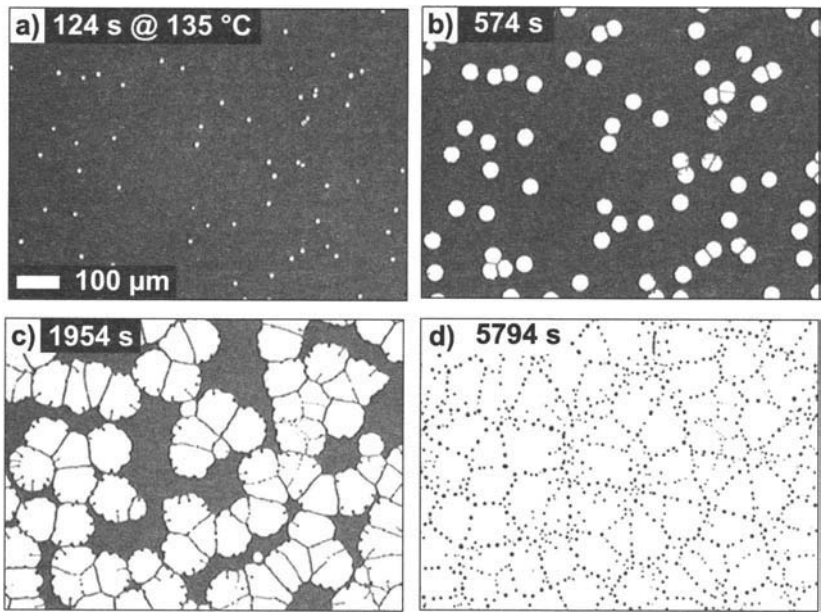

Figure 2. Pictures taken by a light microscope: a 80 nm thick polystyrene film of 65 kg/mol molecular weight is dewetting at 135°C from a hydrophobized silicon substrate. a) t = 2 min, b) t = 10 min, c) t = 33 min, d) t = 97 min.

The clue to the effective interface potential is its connection to the characteristic features of the dewetting pattern. In case $\phi''(h)$ is negative, all fluctuations in film thickness with wavelengths above a certain critical threshold λ_c are amplified and grow exponentially according to $\exp(t/\tau)$, where τ is the growth time that is characteristic for the respective mode which leads to spontaneous dewetting of the liquid (spinodal dewetting). There is, however, a certain wavelength λ_s, the amplitude of which grows fastest, leading to a characteristic dewetting pattern of the liquid film. This spinodal wavelength λ_s is experimentally observable and is linked to the effective interface potential (Vrij, 1966; Ruckenstein and Jain, 1974; Williams and Davis, 1982; Brochard-Wyart

and Daillant, 1989):

$$\lambda_s(h) = \sqrt{\frac{-8\pi^2\sigma}{\phi''(h)}}. \tag{2}$$

This process is analogous to spinodal decomposition of a blend of incompatible liquids which occurs if the second derivative of the free energy with respect to the composition is negative. There, as well, a certain wavelength exists the amplitude of which grows the fastest. Following this analogy, dewetting via unstable surface waves has been termed 'spinodal dewetting' (Mitlin, 1993). Equation (2) illustrates that only if $\phi''(h) < 0$ (spinodal dewetting film), λ_s is real. For $\phi''(h) = 0$, $\lambda_s(h)$ diverges to infinity.

In the metastable case, for a film thickness where $\phi''(h) > 0$, the system has to overcome a potential barrier in order to reach its state of lowest energy at $h = h_{eq}$. Some kind of nucleus, e.g. a dust particle, is required to lower $\phi(h)$ and can therefore induce dewetting. This rupture mechanism is termed 'heterogeneous nucleation' (Mitlin, 1993, 1994). Close to the sign reversal of $\phi''(h)$ it is called 'homogeneous nucleation'. In this case, no nucleus is necessary because the thermal 'activation' is sufficient to overcome the energy barrier (Blossey, 1995).

Equation (2) indicates, that spinodally dewetting films contain experimentally accessible information about the underlying forces and are therefore of special interest. But to make use of equation (2), we first have to prepare a spinodally dewetting film. Our first aim therefore is to unambiguously recognize a spinodally dewetting film. Theoretically, the distinction between nucleation and spinodal dewetting was quite clear: Vrij (1966) proposed already in 1966 that a spinodal rupture of a free liquid film results in a dewetting pattern of 'hills and gullies' with a preferred distance λ_s after a certain time of rupture τ. Experimentally, the rupture time τ is difficult to measure since the hole must have a certain size to be observable. Experimentalists instead concentrated on the evidence of a preferred wavelength λ_s in their systems.

If, however, the holes are randomly (Poisson) distributed, they are assumed to stem from heterogeneous nucleation, reflecting the fact that nuclei typically exhibit random statistics. But in a real experimental system we face a couple of difficulties: the thicker the films are, the weaker is the driving force, and the larger is the growth time τ of the spinodal mode (typically, $\tau \propto h^5$). For thicker films, dewetting by heterogeneous nucleation may therefore be quicker and can suppress a spinodal pattern (Konnur et al., 2000; Becker et al., 2003; Thiele et al., 2001, 2002). Moreover, chemical heterogeneities locally cause a change in ϕ and therefore the rupture conditions of the sample may vary from spot to spot leading to a less ordered dewetting pattern. This effect is more pronounced in thicker films due to the small driving forces and the large growth time τ.

Hence, due to the fact that both nucleation and spinodal dewetting might lead to dewetting in unstable films, the experimental distinction between spinodal dewetting and heterogeneous nucleation is far from being obvious: Experiments referring to the scaling of the preferred hole distance via the spinodal wavelength ($\lambda_s \propto h^2$) and therefore just inferring the average hole density as function of film thickness will very probably fail.

For the distinction between the mechanisms we therefore probe the statistics of the distribution of the sites of the holes. We first determine the simple two-point correlation function $g(r)$ of the point set represented by the positions of the centers of the holes

arising in a dewetting polystyrene film on a hydrophobized silicon substrate, Figure 3(a). Obviously, no feature that indicates a dominant wavelength can be found.

Let us consider for comparison the dewetting pattern of a liquid gold film on a quartz glass, as shown in Figure 3(b) and determine $g(r)$, too. Again, no modulation in $g(r)$ can be detected. For this system, however, spinodal dewetting with a dominant wavelength λ_s had been clearly identified as the dewetting mechanism (Bischof, 1996).

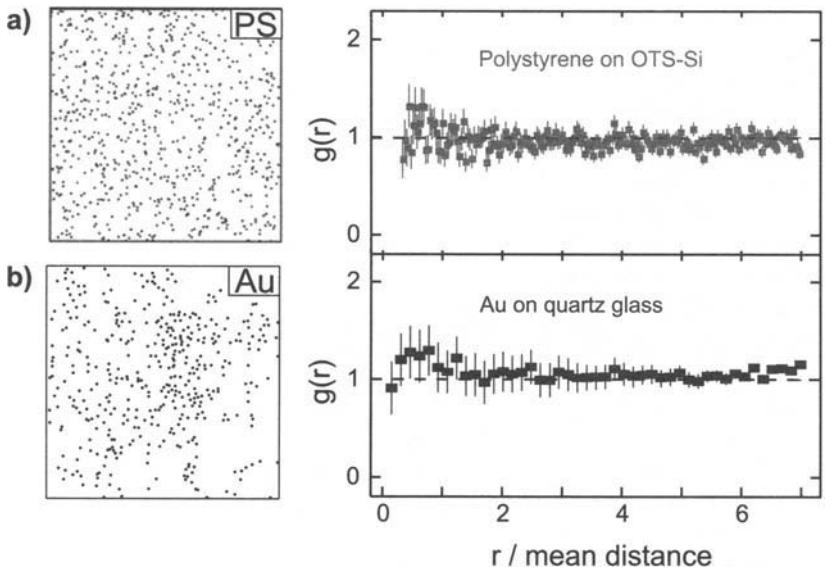

Figure 3. a) Positions of holes in a PS film (left), as extracted from an optical micrograph and the corresponding pair correlation function $g(r)$. b) Position of hole sites in a Au film as extracted from an atomic force micrograph, and as well the corresponding g(r). r is given in units of the mean distance of the holes.

For dewetting patterns where the preferred wavelength cannot be detected by a radial pair correlation function g(r) or a Fourier transform (before the film rupture), more powerful tools have to be applied. Here, Minkowski functionals - based on integral geometrical methods - have shown to be a versatile method to track down higher order correlations (Mecke, 1994; Herminghaus et al., 1998; Jacobs et al., 1998a). Their application to the experimental system of this work is described in detail by Jacobs et al. (2000) in a comparative study on dewetting patterns of gold and of PS films.

The central idea is to determine the spatial statistics of the hole positions by adding a morphology to the point pattern (Mecke, 1994). This is done by assigning circular disks of radius r to each of the hole positions, as shown in Figure 4(a). Due to possible overlap of the disks, the area F and the boundary length U of the set union of disks do not increase proportional with r^2 or r, respectively. The larger the overlap, the slower will be the increase of the two measures. A third Minkowski functional, the Euler characteristics χ, is a measure for the connectivity of a pattern and is defined in two dimensions as the

mean curvature of the boundary line. For a random set of points, the dependence on r of the three Minkowski functionals was analytically determined and then compared with the results obtained for the holes in the gold and in the PS films. The behavior of the Minkowski measures for the holes in the PS films was shown to be in accordance with the result for a random set of holes (Jacobs et al., 1998a); see Figure 4(b). The Minkowski measures for the holes in the gold film, however, differed greatly from the curve of a 'random' sample, demonstrating the presence of correlations between the sites of the holes. This meant that the precondition for a spinodal mechanism was matched for the gold films, but not for PS films on the hydrophobized Si substrates in that study.

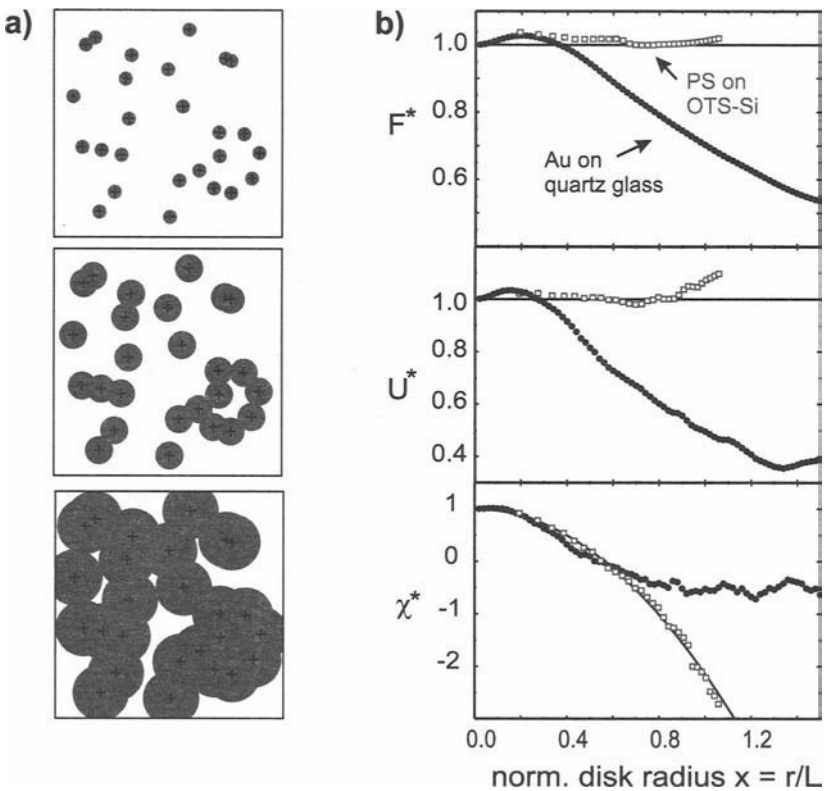

Figure 4. a) The positions of the holes, marked with a cross, are decorated each with a disk, whose radius increases from left to right. The Minkowski functionals in two dimensions include area F (the grey area), boundary length U between grey and white area and the Euler characteristic χ, which is a measure of the connectivity of the grey structure. b) Normalized morphological measures F^*, U^* and χ^* of the Au (full circles) and of the PS film (open squares) as a function of the normalized radius x, $x = 3\mathrm{D}\ r/L$, of the disks with mean distance L. The solid lines mark the expected behavior for a Poisson point process.

The method of determining the Minkowski measures of a point set was applied in all our studies, whenever the presence of correlations between the sites of the holes could not be shown by a Fourier transform or a radial pair correlation function.

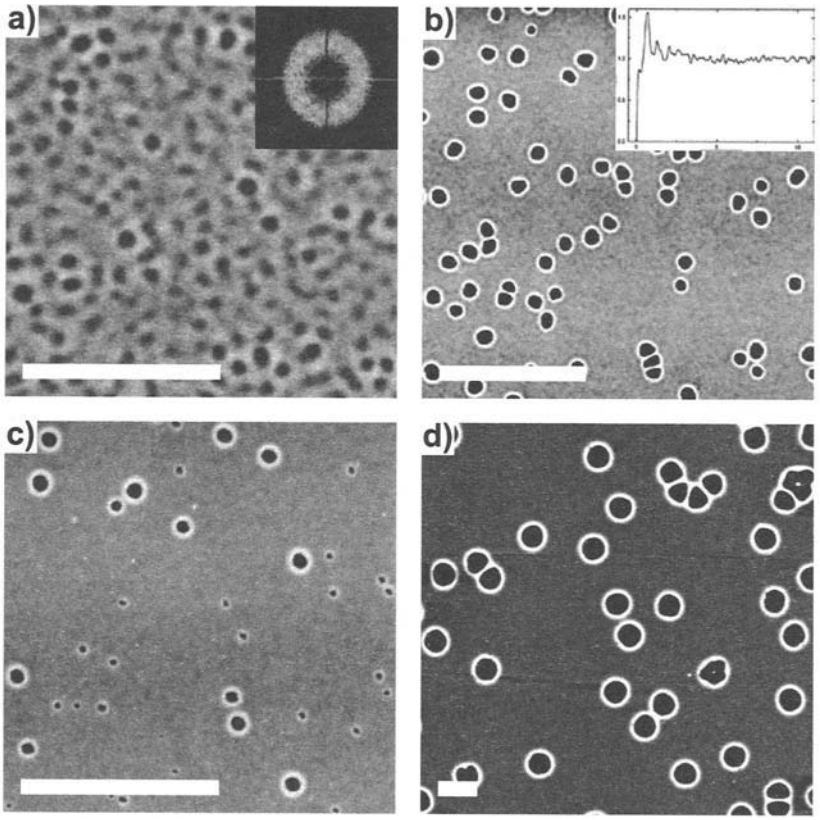

Figure 5. Dewetting patterns of PS(2k) films as seen by AFM; the height scale is ranging from black (0 nm) to white (10 nm; for d) 20 nm). The length bar denotes 5 μm. a) PS film on type C wafer with thickness of 3.9(2) nm, b) 3.9(2) nm PS on type B wafer, c) 4.1(1) nm PS on type B wafer d) 6.6(4) nm PS on type B wafer. Patterns shown in a) and b) are typical for spinodal dewetting, the pattern in c) is characteristic for homogeneous (thermal) nucleation and the pattern in d) stands for a typical scenario of heterogeneous nucleation. (The statistical analysis of the distribution of hole sites in cases b) to d) was performed on larger sample areas.)

In Figure 5, typical snapshots of dewetting patterns are shown. We classify the dewetting patterns into four categories, a representative of each is shown in Figure 2. For the classification we take into account correlations between the sites of the troughs of the undulation: a pattern shown in Figure 5(a) is described as 'densely packed crests and troughs with preferred distance', in Figure 5(b) as 'correlated holes within a uniform

film matrix', in Figure 5(c) as 'randomly distributed holes of different sizes', and in Figure 5(d) as 'randomly distributed holes of one size'.

In Figure 5(a) a 3.9(2) nm thick PS(2k) film dewets from a type C wafer. Many crests and troughs cover the entire film. Some of the troughs are in fact holes since they already touch the substrate. No more uniform film is detectable. A Fourier transform reveals a preferred distance of heaps or bumps, respectively, of 340(30) nm (Seemann et al., 2001a). X-ray diffraction measurements at a later stage of dewetting indicate that the holes are not 'dry'. Rather, they are covered with a residual PS film of thickness 1.3(2) nm. Such a dewetting pattern can be detected up to some 10 nm. For thicker films on that substrate, the time τ until the pattern is sufficiently clear to be observed steeply rises from seconds to months with increasing film thickness ($\tau \propto h^5$). During very long annealing times, however, holes nucleated by e.g. dust particles grow rapidly in size and the entire film is 'eaten up' by those holes before the above described spinodal pattern can develop (Sharma and Khanna, 1998, 1999).

Figures 5(b-d) show a PS(2k) film dewetting from a type B wafer, with increasing film thickness from left to right. Up to a film thickness of 3.9(2) nm, we again observe a preferred distance of holes, but there is still uniform film surrounding the dewetted spots, as shown in Figure 5(b). As compared to PS films on type C wafers, we measure on type B wafers larger preferred distances of holes for the same film thickness. Here, we discover correlations in hole sites either by a ring in the Fourier transform of the image or by observing a modulation within the radial pair correlation function calculated for the sites of holes (Xie et al., 1998; Jacobs et al., 2000; Seemann et al., 2001a). With only slightly thicker PS films, h_o= 4.1(1) nm, the most striking feature is that we observe holes of different sizes within one AFM image and that more and more holes pop up in the course of the experiment, cf. Figure 5(c). Moreover, within the experimental error bar, no correlations of hole sites can be detected. For films of 6 nm thickness and larger, we find a dewetting scenario exemplarily shown in Figure 5(d). Here, we observe isolated circular holes of about identical radius (variance is less than 5%). Upon longer annealing times, these holes grow, but no additional holes emerge.

A detailed analysis with the help of Minkowski functionals reveals that the holes are randomly (Poisson) distributed, as described in an earlier study (Bischof et al., 1996). Up to now, the very nature of the nucleation sites has not been satisfactorily revealed. Already in 1979 Croll found that due to the preparation of thin polymer films from solvents the macromolecular chains are not in an equilibrium state. He found that the stress in a polystyrene film cast from toluene solution at about 20 °C is, quite universally, 14 MPa (Croll, 1979). By annealing the films on a wettable substrate (and thereby most likely reducing the stress inside the films) prior to the transfer to the non-wettable samples, we were able to show that a certain fraction of holes can be suppressed (Podzimek et al., 2001). This has recently been corroborated by Reiter et al. (2005).

By increasing the prepared polymer film thickness on waver type B and C, the dominant wavelength λ_s increases, too, as expected for a spinodal dewetting scenario (Vrij, 1966). Experimental data of $\lambda_s(h)$ are shown in Figure 6(a) as the filled squares. A preferred wavelength λ_s can also be found for PS(2k) films on type B wafers, but only for film thicknesses smaller than 4.1 nm (open circles in Figure 6(a)). On type A and B wafers, PS(2k) films smaller than 3.2 nm could not be prepared by spin coating from

toluene solution, they dewetted during the spin coating process.

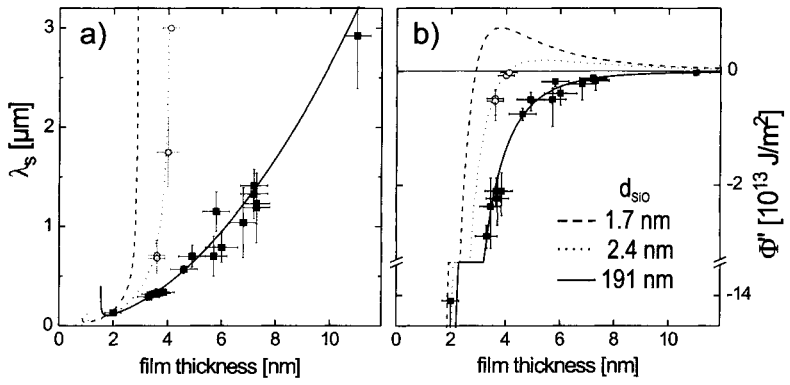

Figure 6. a) Spinodal wavelength λ_s as function of PS film thickness h on type B (open circles) and type C wafers (filled squares). b) Second derivative of effective interface potential ϕ'' as function of film thickness h. Note the axis break of ϕ''.

With the help of equation (2), and using $\sigma = 30.8$ mN/m, we can infer $\phi''(h)$ from $\lambda_s(h)$, as shown in Figure 6(b). In case of a PS film on a type C wafer, a simple van der Waals potential of the form

$$\phi_{vdW}(h) = -A_{SiO}/(12\pi h^2), \tag{3}$$

can be fitted to the data of $\phi''(h)$ (Figure 6(b), solid line). A_{SiO} is the Hamaker constant for a PS film on a SiO substrate. Here, A_{SiO} is a fit parameter with the value A_{SiO}= 2.2(4) E^{-20} J, which is in excellent agreement with the Hamaker constant calculated by refractive indices and dielectric constants of the materials in the layered system air/PS/SiO (Israelachvili, 1992): $A_{SiO,calc}$= 1.8(3) E^{-20} J.

Since a van der Waals potential, as shown in equation (3), cannot explain a global minimum of $\phi(h)$ at the equilibrium film thickness h_{eq}, we introduce a model potential that additionally contains a $1/h^8$ dependence, which is one of the models commonly used in this context:

$$\phi(h) = c/h^8 + \phi_{vdW}(h). \tag{4}$$

Here, the first term includes short range interactions of strength c and the second term characterizes the long-range interactions by the van der Waals potential.

$\phi(h)$ has to fulfill two further conditions which define the position and depth of the global minimum, $\phi(h_{eq})$. First, the contact angle θ of the liquid on the substrate, which can be determined independently by AFM (7.5° in our case), fixes the depth of the global minimum, equation (1). Second, the position h_{eq} of the global minimum is determined by the equilibrium film thickness of 1.3(2)nm as measured by X-ray reflectivity. We found that by a suitable choice of the free parameter c, both conditions can be fulfilled. We obtain c = 6.3(1) E^{-76} Jm^6 for a 191 nm SiO layer. The reconstructed effective interface

potential is plotted as solid line in Figure 3. For all experimental film thicknesses (< 60 nm) $\phi''(h)$ is negative and therefore the PS films on type C wafers are unstable.

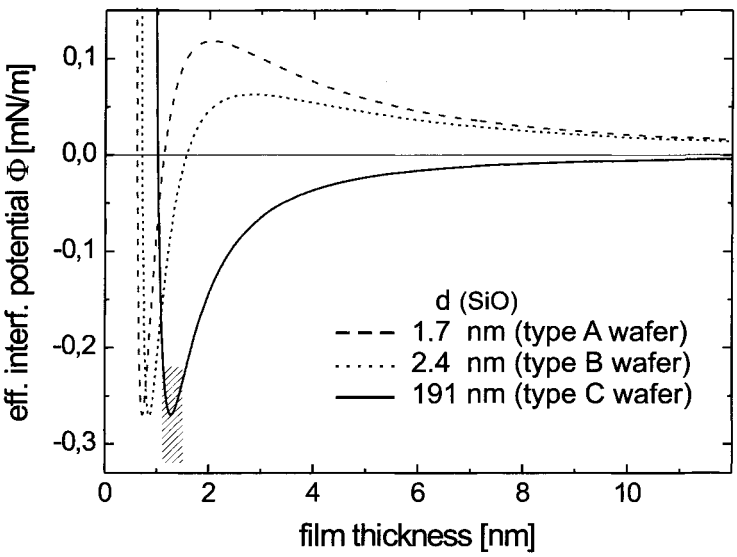

Figure 7. Reconstructed effective interface potential $\phi(h)$ for polystyrene films on three types of silicon wafers. The hatched rectangle indicates in x-direction the experimental error for h_{eq} from the X-ray measurements, and in y-direction the error in $\phi(h_{eq})$ due to the limited accuracy of the contact angle measurement.

Up to now, we treated the PS films on type C wafers as a 'two interfaces'-system, air/PS/SiO, and neglected the bulk silicon underneath the SiO. For type A and B wafers, however, with oxide layer thicknesses of only 1.7 nm and 2.4 nm, respectively, this approximation turns out not to be adequate. These have to be treated as 'three interfaces' systems, air/PS/SiO/Si. This may be done by considering the van der Waals potential of the PS film to be composed of two terms: one of the SiO layer and one of the silicon bulk corrected by the SiO layer thickness d:

$$\phi_{vdW}(h) = -\frac{A_{SiO}}{12\pi h^2} + \frac{A_{SiO} - A_{Si}}{12\pi(h+d)^2}. \tag{5}$$

It is one of the aims of the discussion below to test the adequacy of this procedure.

In case of type B wafers, we now apply the same procedure for reconstructing $\phi(h)$ as before, but use equation (5) instead of equation (3) for $\phi_{vdW}(h)$. By fitting the second derivative of equation (5) to the experimental data for $\phi''(h)$ in Figure 6(b) and using the Hamaker constant A_{SiO} from above, we obtain A_{Si} = -1.3(6) E^{-19} J. That again corresponds very well to the calculated value of $A_{Si,calc}$= -2.2(5) E^{-19} J. Following the

procedure as described before, we obtain a strength c of the short range attraction of $c = 5.1(1)\ \mathrm{E}^{-77}\ \mathrm{Jm}^6$ for a 2.4 nm SiO layer. $\phi(h)$ is plotted as dotted curve in Figure 7. For films thicker than 4.1 nm, $\phi''(h)$ is positive and thus dewetting will only proceed by nucleation, whereas for thinner films spinodal dewetting is possible. Both are consistent with our experimental observation on type B wafers.

For PS films on type A wafers, we can now reconstruct $\lambda_s(h)$ even without any experimental data points for λ_s: the long-range part of $\phi(h)$ can be calculated by equation (5) with $d = 1.7$ nm and the Hamaker constants mentioned before. The short-range part can be obtained by relating the experimental contact angle θ to the global minimum of ϕ via equation (4) and choosing the strength c adequately. We find $c = 1.8(1)\ \mathrm{E}^{-77}\ \mathrm{Jm}^6$. Here again, $\phi(h)$ describes a metastable PS film (cf. Figure 7, dashed line) and $\phi''(h)$ is positive for PS films thicker than 2.9 nm, which is consistent with our experiments, where we observe only nucleated holes for films thicker than 3.2 nm. This is different with earlier work using silicon wafers with a native oxide layer as a substrate (Xie et al., 1998). In that work, patterns reminiscent of spinodal dewetting were observed for PS thicknesses up to 10 nm. According to our findings, this can never be achieved with a native oxide layer. Furthermore, no agreement was reached between the calculated and experimental Hamaker constant.

From the reconstructed effective interface potentials for all three types of substrates we can infer the particular dependence of the spinodal wavelength λ_s on PS film thickness h via equation (2). All three $\lambda_s(h)$ curves are plotted in Figure 6(a). The results of these experiments are summarized in Figure 8. Films that exhibit patterns with a structure factor are marked as open symbols. Systems with only randomly distributed holes are given solid symbols. A star marks a situation as described in Figure 5(c), where more and more holes pop up in the course of the experiment. (The single star-shaped point in Figure 8 comprises three data points lying on top of each other.) The three types of wafers are identified by triangles (type A), circles (type B), and squares (type C). These experimental results can be understood in terms of the reconstructed effective interface potential $\phi(h)$ (Seemann et al., 2001a), that is shown in Figure 7.

From the potentials we can infer the thickness $\tilde{h}$ below which $\phi''(h)$ is negative and spinodal dewetting is possible: for type A wafers, $\tilde{h} = 2.9(3)$ nm and for type B wafers, $\tilde{h} = 4.1(3)$ nm. Here, the error bars account for the errors determining the oxide layer thicknesses and the Hamaker constants involved. For type C wafers, $\tilde{h} = 325$ nm as determined from the potential shown in equation (5). Accounting again for the error in $\phi(h)$ due to the involved Hamaker constants, $\tilde{h}$ is within the interval 230 nm $< \tilde{h} <$ 495 nm. Experimentally, this relatively large error interval is nevertheless irrelevant, since an estimation of the spinodal rupture time τ of an even 230 nm thick PS(2k) film on type C wafer gives values for τ larger than 2000 years [1]. In other words, spinodal dewetting on Si/SiO substrates is observable under lab conditions for PS film thicknesses below 15 nm only. Otherwise, as described before, heterogeneous nucleation will always be faster in initiating holes.

[1] For the estimation of τ we used equation (31) of Sferrazza et al. (1998), $\tau = 48\pi h\sigma h^5/A^2$ with viscosity $h = 3200$ Pa s, surface tension $\sigma = 31$ mN/m and a Hamaker constant A of SiO_x of $A = 2.2$ E-20 J, taken from Seemann et al. (2001a).

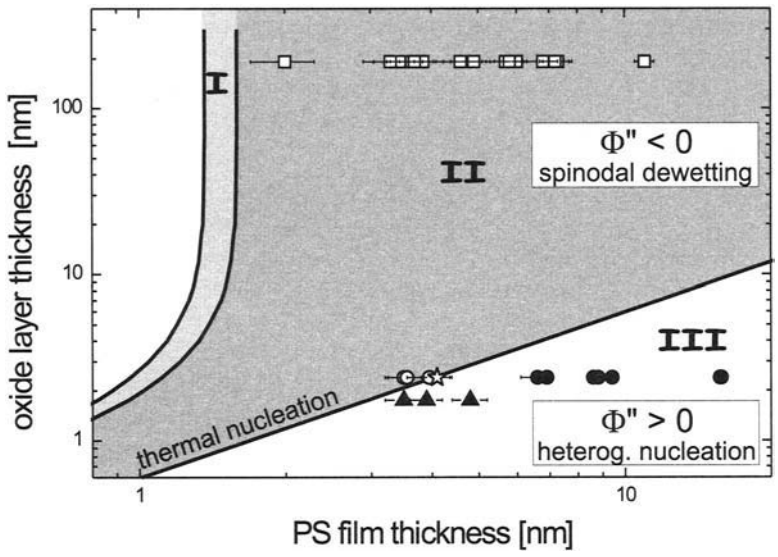

Figure 8. Stability diagram of PS films on top of silicon wafers with variable oxide layer thickness. Experiments that exhibit patterns with a structure factor (e.g. Figure 5(a) and (b) are marked as open symbols. Systems with only randomly (Poisson) distributed holes (e.g. Figure 5(d)) are given solid symbols. A star marks a situation as described in Figure 5(c). The three types of wafers used in the experiments are identified by triangles (type A), circles (type B), and squares (type C). In the grey areas, regimes I and II, PS films can dewet by a spinodal mechanism, in regime III only heterogenenous nucleation is possible.

With the help of the equation (5) for the effective interface potential $\phi(h)$, we are now able to predict stability conditions of PS films on Si/SiO substrates: From the reconstructed $\phi(h)$ we can infer the zero of $\phi''(h)$ as a function of oxide layer and PS film thickness. This curve is plotted in Figure 8 [2]. It hence separates the spinodal regime II (dark gray area) from the regime III of heterogeneous nucleation (bright area) and may be called 'spinodal line' [3]. Along the spinodal line, homogeneous nucleation by thermal fluctuations is possible (Blossey, 1995). The region of thermal nucleation is very narrow, effectively collapsing to a single line in this graph. For silicon wafers without any oxide layer, equation (5) predicts PS films to be stable. This, too, is found experimentally

[2]It should be pointed out that in the unstable regimes I and II as well as in the metastable regime III, heterogeneous nucleation is possible and indeed is observed as explained later in the text, but spinodal dewetting can only take place in regimes I and II.

[3]The spinodal line here is analogous to the spinodal line separating the metastable and the spinodal (unstable) region in the phase diagram of the decomposition of two incompatible liquids.

(Stange et al., 1997; Jacobs et al., 1998b), if the oxide layer is stripped away (e.g. by an HF dip) prior to PS film preparation.

Let us now compare the experimental data points plotted in Figure 8 with the regimes predicted by the effective interface potential of equation (2). In regime II, data points with open symbols are found, which account for the fact that a spinodal wavelength λ_s was observed and measured. These data of λ_s were used to reconstruct the interface potentials shown in Figure 7. It is therefore obvious that in regime II only open symbols are found. Filled symbols stand for experiments were randomly dispersed holes were detected. From these experiments, we cannot reconstruct ϕ. Nevertheless, all of the filled data points, measured on type A and B wafers, are located in regime III. Hence, the reconstructed effective interface potentials correctly predict the dewetting behavior even in these cases. Of particular interest in this context are the experiments on type B wafers. The stability diagram in Figure 8 predicts that for $h < \tilde{h} = 4.1(1)$ nm spinodal dewetting is possible, whereas for thicker films, nucleation is the only dewetting mechanism. This exactly corroborates our experimental findings. Close to the sign reversal of $\phi''(h)$ at $h = \tilde{h} = 4.1(1)$ nm, thermal nucleation is predicted. Indeed, typical signs of thermal nucleation are experimentally observed: holes are generated during the entire dewetting process and the sites of the holes are not correlated. Hence, on type B wafers, all three types of rupture mechanisms are theoretically predicted and experimentally observed.

It is now challenging to compare our results with simulations of dewetting patterns of Sharma and Khanna (1998, 1999). They proposed that the morphology of the dewetting pattern depends on the form of the effective interface potential at the present film thickness h, or, more precisely, on the course of $\phi''(h)$. To explain this in more detail, the effective interface potential $\phi(h)$ and its second derivative $\phi''(h)$ are sketched in Figure 9 for an unstable (a) and for a metastable film (b) as function of film thickness h. For both systems, the global minimum of $\phi(h)$ is at finite film thickness h_{eq}. We divided the course of the effective interface potential now into three regimes, following a suggestion of Sharma and Khanna (1998, 1999). Regimes II and III are defined as before in Figure 8 and differ in the sign of $\phi''(h)$. In regime I, $\phi''(h)$ is negative, too, and the film can spinodally dewet, but $|\phi''(h)|$ is decreasing with decreasing film thickness, whereas in regime II it is increasing. The results of the simulations of Sharma and Khanna in regime I and II are shown in Figure 9(c) and 9(d), respectively. In regime I, Figure 9(c), the formerly uniform film has been transformed into a landscape of only crests and troughs, whereas in regime II, Figure 9(d), isolated holes can be found within a matrix of still uniform film. Sharma and Khanna explain this considerable difference in behavior by the course of $|\phi''(h)|$, which acts as a kind of driving force for the instability. In regime II, deep troughs (meaning sites of small PS film thickness) experience a stronger driving force than shallow ones, whereas it is vice versa in regime I. Therefore, in regime II single holes in a film matrix are prevailing, yet in regime II shallow troughs also may lead to holes, resulting in a 'crests and troughs' pattern morphology. In regime III, where only nucleation is possible, the holes in the film will be distributed according to the statistics of the nuclei. In Figure 9(e), a Poisson distribution of 40 nuclei or holes, respectively, is depicted.

To compare qualitatively our experimental dewetting patterns with the ones of Sharma and Khanna's simulations, we assign a pattern like the one in Figure 5(a) with a simu-